RSC Advances

ROYAL SOCIETY OF CHEMISTRY

www.rsc.org/advances

Fluorescent cyclodextrin carriers for a water soluble Zn^{II} pyrazinoporphyrazine octacation with photosensitizer potential

R. Anand,[1] F. Manoli,[1] I. Manet,[1] M. P. Donzello,[2] E. Viola,[2] M. Malanga,[3] L. Jicsinszky,[3] E. Fenyvesi,[3] S. Monti[1]*

[1] *Istituto per la Sintesi Organica e la Fotoreattività, Consiglio Nazionale delle Ricerche , via P. Gobetti 101, I-40129 Bologna, Italy*

[2] *Dipartimento di Chimica, Università degli Studi di Roma "La Sapienza", P.le A. Moro 5, I-00185 Roma, Italy*

[3] *CycloLab, Cyclodextrin R&D Ltd., Illatos út 7, H-1097 Budapest, Hungary*

Abstract

A nitro-benzofurazan-triazolyl carboxymethylated β-cyclodextrin (NBFT-CMβCyD) and an oligomer of carboxymethyl β-cyclodextrin (sodium salt), crosslinked with epichlorohydrin and labeled with rhodaminyl groups (pβCyD-Rh), exhibit very high affinity in aqueous solution for the octacationic photosensitizer $[(CH_3)_8LZn]^{8+}$ neutralized by I^- ions (L = tetrakis-2,3-[5,6-di(2-(pyridiniumyl)pyrazino]porphyrazinato dianion). The photosensitizer (PS) forms complexes with 1:2 and 2:2 CyD:PS stoichiometry, which have been characterized as to binding constants and UV-Vis absorption and fluorescence properties. The selfassociation tendency of $[(CH_3)_8LZn]^{8+}$, leading to a monomer-dimer equilibrium shifted toward the dimer even at very low concentrations ($\approx 10^{-6}$ M), is not contrasted by either NBFT-CMβCyD or the pβCyD-Rh oligomer, both of which completely convert the $[(CH_3)_8LZn]^{8+}$ monomer fraction to the dimer form in the bound state. Quenching of

fluorescence observed in $[(CH_3)_8LZn]^{8+}$ upon binding with either hosts is consistent with conversion of the monomer to the negligibly fluorescent dimer. The complexes formed with the CMβCyD units of the pβCyD-Rh oligomer have average association constants larger by 6-7 order of magnitudes than those with the CMβCyD monomer in the NBFT-labeled derivative.

Corresponding Author:

Dr. Sandra Monti, FRSC
CNR -Istituto per la Sintesi Organica e la Fotoreattività (ISOF)
Via P. Gobetti 101
I-40129 Bologna, Italy
tel ++39 051 639 9813
fax ++39 051 639 9844
e-mail address: sandra.monti@isof.cnr.it

Introduction

A class of macrocyclic compounds recently attracting a lot of interest are phthalocyanine analogues with heterocyclic rings annulated to the pyrrole moieties of the porphyrazine core.[1, 2] Their UV-Vis spectroscopic and photophysical properties recall those of the parent phthalocyanines, whereas redox behavior is affected by the nature of the peripheral heterocyclic rings, making stepwise one-electron reductions to occur at less negative potentials than in the parent phthalocyanines [3-6] Because of their unique features such porphyrazine derivatives received considerable attention for technological, catalytic and biomedical applications.[2]

Several pyrazinoporphyrazines, both free-base and metal complexes, were recently synthesized and characterized.[4-6] Some of them generate singlet oxygen with good yields, thereby representing promising materials for photodynamic therapy (PDT) and antimicrobial treatment.[7, 8] Introduction of positively charged groups rendered them soluble in water mainly in aggregated form. Multimodal anticancer potentialities emerged for some of these water soluble cationic derivatives.[9-11] While the presence of cationic functional groups favours solubilisation in water, high charge density conditions cellular uptake and localization in sub-cellular compartments, not always favouring membrane penetration.[12, 13] Development of suitable carriers is thus expected to improve the performances of the photosensitizers reducing, for example, selfassociation tendency and allowing more selective and efficient accumulation in cancer tissues. The development of photosensitizer-carrier systems (“third generation photosensitizers”) represents nowadays one of the frontiers in the design of photosensitizers for PDT.[14]

In this work we focused our attention on the water soluble octacationic tetrakis-2,3-[5,6-di(2-(*N*-methyl)pyridiniumyl)pyrazino]porphyrazinato-Zn^{II} in the form of iodide salt ($[(CH_3)_8LZn]^{8+}$, see Scheme 1A).[5, 6] This molecule is an efficient singlet oxygen sensitizer and possesses a large positive charge that can be beneficial for interaction with negatively charged phosphate groups of nucleic

acids and outer membrane of Gram-negative bacteria or negatively charged fungal cell walls.[12, 15] Its ability to bind to G-quadruplex and B-DNA has been also proved in solution.[7, 10, 11] Although aggregation phenomena have been observed in water, $[(CH_3)_8LZn]^{8+}$ is present in monomeric form in non aqueous, low-donor solvents.[5]

We considered cyclodextrin (CyD) derivatives as complexing agents with carrier function. CyDs are biocompatible cyclic oligosaccharides, made of α-D-glucopyranose units joined by α(1-4) linkages. They possess a torus-shaped structure with a hydrophilic external surface and a hydrophobic cavity able to form host-guest complexes. CyD-based host systems have been proposed in both clinical and preclinical studies for improved delivery of drugs [16] and porphyrin photosensitizers. [17] In particular crosslinked CyD polymers spontaneously assembling into nanoparticles [18] have different binding sites, i.e. amid the 3D macromolecular network and within the CyD cavities, thereby enhancing the apparent solubility and regulating the self-association tendency of drugs. [19, 20] Moreover this kind of hosts can be implemented for multimodal applications in the biomedical field. For example an epichlorohydrin crosslinked β-CyD polymer can be made photoresponsive and applicable for both imaging and therapy upon co-encapsulation of suitable chromophoric units. [21]

Considering the positive performances of β-CyD-based polymers as carriers for photoactivatable prodrugs we have explored the binding modes of $[(CH_3)_8LZn]^{8+}$ to two fluorescent β-CyD systems, a CyD monomer (Scheme 1B) and a CyD crosslinked oligomer (Scheme 1C) with the aim to optimize transport of cationic pyrazinoporphyrazine photosensitizers. Both the investigated CyD derivatives possess covalently attached units: i) carboxylate groups, mainly on the CyD secondary side, expected to play a role in the recognition of the photosensitizer and ii) fluorescent labels, e.g. a nitro-benzofurazan-triazolyl chromophore on the primary side of the CyD monomer and a rhodaminyl moiety randomly attached to the CyD oligomer. Compared to CyD-

based carriers binding non covalently fluorescent probes, intrinsically fluorescent CyDs have a more general interest because their detection in solution and in cellular environments is free from drawbacks due to fluorescent probe dissociation.[22] In both the monomeric and the oligomeric CyD hosts the negatively charged carboxylate groups were reasonably expected to influence the affinity for the photosensitizer, whereas the fluorescent labels were expected to allow for probing.

The complexation process was studied performing accurate titrations with UV-vis absorption and fluorescence monitoring. Multiwavelength spectroscopic data taken at different host concentrations were analyzed with global methods to determine the stoichiometry, formation constants and spectral features of the complexes. A further goal of the study was indeed to test the ability of the adopted experimental and computational approach to provide information on the interaction of the photosensitizer to the CyD systems. A detailed quantitative and qualitative picture of the binding of $[(CH_3)_8LZn]^{8+}$ with the negatively charged CyDs was obtained. Both hosts revealed unsuited for monomerization of this guest. However, the adopted methods proved to be useful to shed light onto the interaction of selfassociating macrocyclic compounds with CyD systems with either monomeric or polymeric structure.

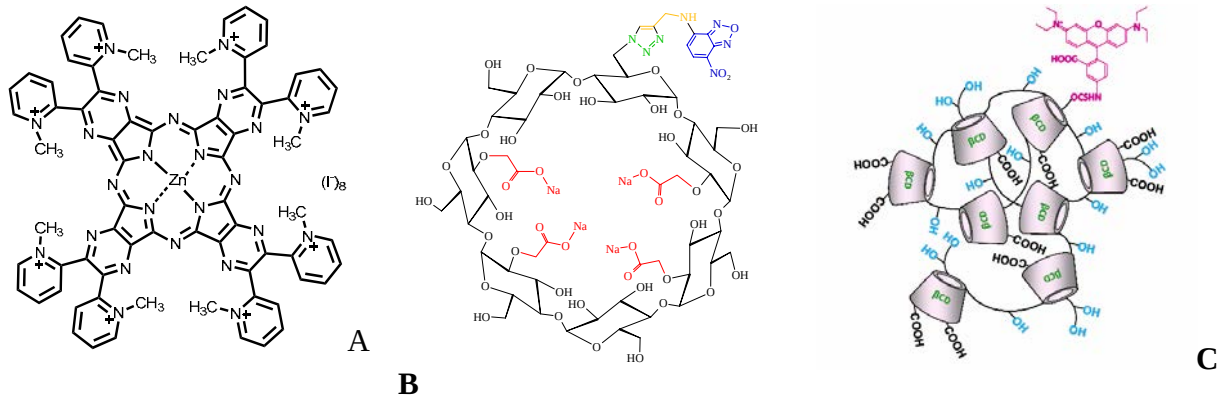

Scheme 1. (A) The octacation ($[(CH_3)_8LZn]^{8+}$) (L = tetrakis-2,3-[5,6-di(2- (pyridiniumyl)pyrazino]porphyrazinato dianion). The cationic porphyrazine is neutralized by I^- ions; (B) nitro-benzofurazan-triazolyl carboxymethylated β-cyclodextrin (NBFT-CMβCyD) (C) Oligomer of carboxymethyl β-cyclodextrin sodium salt labeled with rhodaminyl groups (pβCyD-Rh), COOH groups are mainly connected to the secondary side and rhodaminyl moiety is randomly connected to tthe cyclodextrin unit.

2. Experimental section

Materials

The octacation ($[(CH_3)_8LZn]^{8+}$) (neutralized by I- ions; L = tetrakis-2,3-[5,6-di(2-(pyridiniumyl)pyrazino]porphyrazinato dianion) was synthesized as reported previously.[5] Nitro-benzofurazan-triazolyl carboxymethylated β-cyclodextrin (NBFT-CMβCyD) was prepared according to the procedure described below. The oligomer of carboxymethyl β-cyclodextrin sodium salt crosslinked with epichlorohydrin and labeled with rhodaminyl groups (pβCyD-Rh) was obtained by reacting carboxymethyl β-cyclodextrin with 1-chloro-2,3-epoxy propane and then Rhodamine B isothiocyanate, as described by Puskas *et al*.[23] The oligomer used has a molecular weight of 44 kDa, Degree of substitution (DS) for rhodaminyl groups ca. 0.3-0.4 per oligomer, DS for COONa ca. 2.5 per CyD unit. 6-monoazido-6-monodeoxy-β-CyD was a fine chemical product from CycloLab. All the reagents and solvents were from Sigma-Aldrich. Water was purified by Millipore Milli-Q system, Millipore SpA, Milan, Italy.

Synthesis and characterization of β-CyD derivatives

6-Monodeoxy-6-monoazido-carboxy-methyl-β-CyD sodium salt (CMβCyD). Sodium chloroacetate (300 g, 2.57 mol) was dissolved in water (1 L) and 6-monoazido-6-monodeoxy-β-CyD (580 g, 0.5 mol) was gradually added to the stirred solution. The white suspension was heated at 60 °C and water (300 mL) solution of NaOH (120 g, 3 mol) was added dropwise (in a period of 2 h) keeping the temperature strictly under 70 °C. The reaction mixture was further heated at 70 °C for 4 h, concentrated under reduced pressure (T = 60 °C) to 1/3 of volume and then poored to EtOH (5 L) under sonication. The suspension was decantated and EtOH (1 L) was added to the sticky white material under sonication. This procedure was repeated three times, then the white solid was dissolved in water (1 L), anionic (200 g) and cationic (20 g) resins exchange were added and the

solution was stirred for 2 h. The resins were filtered off, charcoal (50 g) was added to the solution, the suspension was stirred for 1 h, filtered and membrane filtered. The pH of the resulting solution was set to 8-9 with NaOH (3 M) and freeze drying yielded the product as white powder (518 g, 74 %). IR, ^{1}H-NMR and ^{13}C-NMR features are listed below and spectra are given in ESI-1-Figure S1. Degree of substitution (DS) for carboxymethyl groups was 3-4.

IR (KBr) ν/cm^{-1}: 3398 (O-H), 2927 (C-H), 2104 (N_3), 1605 (COO^-), 1419 (C-C/C-O stretch), 1327, 1246, 1161, 1085, 1031, 948, 846, 757, 710, 582, 534.

^{1}H-NMR (D_2O): δ 3.40-4.40 (br m, 49H, H2, H3, H4, H5, H6, $\underline{CH_2}$-COOH), 5.05 (br s, 4H, H1), 5.27 (br s, 3H, H1).

^{13}C-NMR (D_2O): δ 54.00 (C6-N3), 60.66 (C6), 70.58 ($\underline{CH_2}$-COO^-), 71.41, 71.61, 71.96, 73.20, 80.86, 99.66 (C1'), 101.63 (C1), 177.75 (CO), 178.91 (CO). (for more detailed assignment see HSQC-DEPT spectrum in ESI-1-Figure S1).

Mono-4-(N-propargyl)-7-nitrobenzofuran. The synthesis of this compound was already described.[24] We adopted anyway modified conditions in the synthesis. Propargylamine (0.13 mL, 2.0 mmol) was diluted with CH_3CN (10 mL), the solution was cooled down (T= 5 °C) and 4-chloro-7-nitrobenzofurazan (200 mg, 1.0 mmol) dissolved in CH_3CN (2 mL) was added dropwise (10 min addition). The reaction mixture was stirred for 1 h, the crude was filtrated and extensively washed with CH_3CN to yield mono-4-(N-propargyl)-7-nitrobenzofuran as brown powder (166 mg, 76 %).

^{1}H NMR ($CDCl_3$): δ=2.43 (t, 1H), 4.29 (dd, 2H), 6.30 (broad, 1H, NH), 6.33 (d, 1H), 8.53 (d, 1H) (in accordance with literature data).[24]

ES-MS in positive ionization mode calcd. m/z = 218.0297, found $(M+H)^+$ = 219.0235 (see ESI-1-Figure S2).

Nitrobenzofurazan-NH-triazolyl-carboxymethyl-β-CyD (NBFT-CMβCyD). The 6-monodeoxy-6-monoazido-carboxymethyl-β-CyD sodium salt (0.74 g, 0.5 mmol, DS = 3-4 for carboxymethyl) was dissolved in 20 mL H_2O:DMF (96 %) 8:2 (v/v); mono-4-(N-propargyl)-7-nitrobenzofuran (0.22 g, 1 mmol), $CuSO_4 \cdot 5H_2O$ (0.25 g, 1 mmol) and sodium ascorbate (0.2 g, 1 mmol) were added and the reaction mixture was stirred for 20 h at room temperature (see scheme 2).

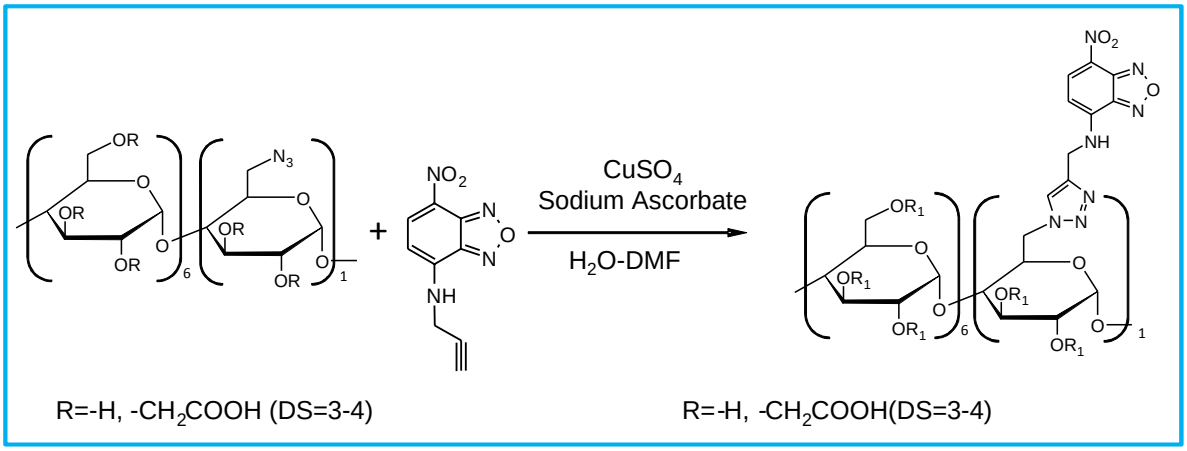

Scheme 2. Fluorescent labeling of 6-monodeoxy-6-monoazido-carboxymethyl-β-CyD sodium salt. Reaction scheme

The solution was treated with both cationic and anionic ion exchange resin, the resin was filtered off and the filtrate was precipitated with acetone (30 mL). The solid was dissolved in H_2O, the pH was set between 7-8 and freeze drying yielded the final product as a pale brown solid (0.72 g, 84%). IR, ^{1}H-NMR, ^{13}C-NMR and HR-MS features are listed below and the spectra with the detailed assignments are given in ESI-1-Figure S3. Degree of substitution (DS) for the fluorescent tag was ~ 1.

IR (KBr) ν/cm^{-1}: 3382 (O-H), 2928 (C-H), 1601 (COO^-), 1421 (C-C/C-O stretch), 1318, 1157, 1109, 1034, 949, 843, 758, 707, 615, 585.

^{1}H-NMR (D_2O): δ= 3.34-4.84 (bs, 51H, H2, H3, H4, H5, H6, O-$\underline{CH_2}$-COOH, C-$\underline{CH_2}$-NH), 5.06 (bs, 5H, 1H), 5.28 (bs, 2H, H1), 6.54 (bs, 1H, aromatic-H), 7.92 (s, 1H, H-triazole), 8.11 (bs, 1H, aromatic-H).

^{13}C-NMR (DMSO-d_6):δ= 54.22 (C6-N), 62.04 (C6), 76.20 ($\underline{CH_2}$-COO^-), 79.67, 100.15 (C1), 101.38 (C1'), 123.91, 124.98, 129.44, 132.48, 138.64, 144.85, 164.16, 164.83, 165.70, 181.78 (CO).

(for more detailed assignment see HSQC-DEPT spectrum in ESI-1-Figure S3).

Spectroscopic measurements

All the measurements were carried out at 295 K. ^{1}H-, HSQC-DEPT, ^{13}C-and APT-NMR spectra were recorded on a Varian VXR-600 at 400 or 600 MHz. IR spectra were recorded in KBr disk on a Nicolet 205 FTIR. MS spectra were obtained on a Agilent 6230B TOF LC/MS system. UV-Vis absorption spectra were recorded on a Perkin-Elmer lambda 650 spectrophotometer in 1 cm quartz cuvette with water as the reference. Circular dichroism (CD) spectra were obtained with a Jasco J-715 spectropolarimeter. Each CD spectrum was registered by accumulating 3 scans with an integration time of 1 s; scan rate was 50 nm/min for the whole range. Fluorescence spectra were obtained on an Edinburgh FLS 920 Fluorimeter (continuous 450 W Xe lamp for excitation), equipped with a Peltier-cooled Hamamatsu R928 photomultiplier tube for detection in right angle mode. Fluorescence lifetimes were measured in air-equilibrated solutions with a time correlated single photon counting system (IBH Consultants Ltd.). Nanosecond LED sources at 373, 465 or 560 nm were used for excitation, and the emission was collected at right angle with suitable long pass cutoff filters. Decay profiles were analysed using a multiexponential function (eq.1) and deconvolution of the instrumental response. The software package was provided by IBH Consultants Ltd.

$$I(t) = \Sigma_i a_i \times \exp(-t/\tau_i) \qquad (1)$$

Global analysis methods

Titration experiments with absorption or fluorescence monitoring were performed at constant concentration of either component. The best complexation model and the related association

constants were determined by global analysis of multiwavelength data sets corresponding to 10-15 spectra of different mixtures, using the SPECFIT/32 program (version 3.0.40, TgK Scientific). The program uses a multivariate optimization procedure based on singular value decomposition (SVD) and non linear regression modeling by the Levenberg−Marquardt algorithm. The deviations of the calculated spectroscopic quantities from the experimental values are minimized in a completely numerical procedure. See the ESI-3 for further details.

3. Results and discussion

Self-aggregation of $[(CH_3)_8LZn]^{8+}$

The UV-visible absorption spectrum of $[(CH_3)_8LZn]^{8+}$ in water (ESI-2-Figure S4) is characterized by a Q band system with two maxima of comparable intensity at ca. 625 and 655 nm, attributed to the existence of a monomer-dimer equilibrium with log (K_d/M^{-1}) = 7.1. [10, 11] The peak at longer wavelength is assigned to the monomeric species. Indeed, as already reported,[11] $[(CH_3)_8LZn]^{8+}$ in the presence of sodium dodecylsulfate (SDS) micelles exhibits a major peak at ca. 660 nm assigned to the monomer, dominating thanks to association of the octacationic macrocycle to the negatively charged micelle surface. The monomerization of the octacation by the negatively charged micellar environment proned us to test the negatively charged cyclodextrin derivatives as carriers.

The fluorescence properties of $[(CH_3)_8LZn]^{8+}$ are also strongly affected by selfaggregation. The emission spectrum is characterized by a peak at 670 nm and a shoulder at 750 nm and is assigned mainly to the monomeric species with lifetime of ca. 2.52 ns, whereas the dimer has a subnanosecond lifetime and does not contribute appreciably to the steady state emission intensity (see Table 1).[11]

Spectroscopic properties of NBFT-CMβCyD

The UV-Vis absorption, fluorescence and circular dichroism (CD) spectra of the NBFT-CMβCyD host in water are shown in Figure 1. The absorption and emission spectra are characterized by maxima at 467 and 537 nm, respectively. The measured fluorescence lifetime is 1.4 ns (Table 1). The CD signal observed above 240 nm and extending into the visible indicates the presence of a CyD-induced ellipticity in the lowest energy electronic transitions of the dye.

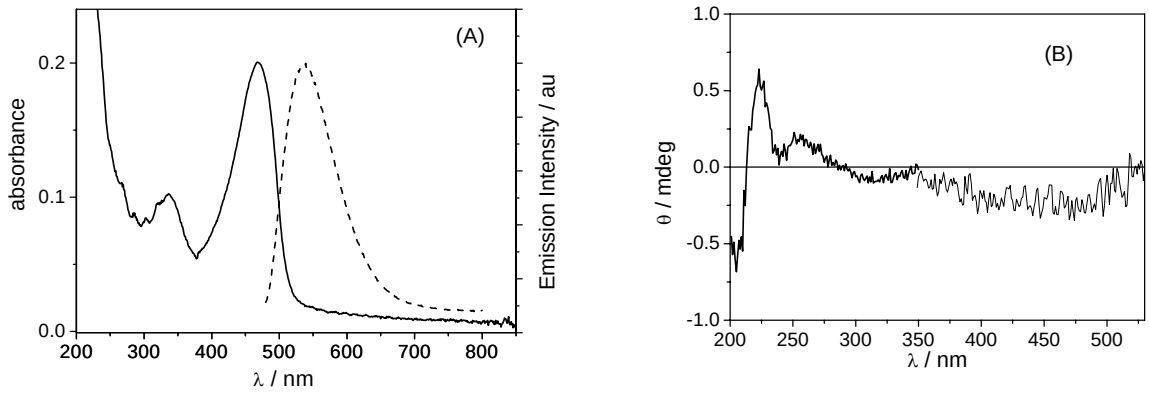

Figure 1. NBFT-CMβCyD 4.0 $\times 10^{-5}$ M in water: (A) Uv-Vis absorption (solid, cell path length 1cm) and emission (dashed, λ_{exc} = 470 nm, uncorrected); (B) Circular dichroism spectrum (200-350 nm, cell path length 2 cm, 350-560 nm, cell path length 1 cm).

Table 1. Fluorescence properties of NBFT-CMβCyD, pβCyD-Rh oligomer and $[(CH_3)_8LZn]^{8+}$ in water, T= 22 °C.

	Exc/nm	**Em/nm**	**(a_1) τ_1/ns**[a]	**(a_2) τ_2/ns**[a]	
NBFT-CMβCyD	465	539	(1.00) 1.40		$\chi^2 = 0.80$
$[(CH_3)_8LZn]^{8+}$	373	670	(0.15) 0.37	(0.85) 2.52	From ref.[11]
pβCyD-Rh	560	575	(0.65) 1.03	(0.35) 2.60	χ^2 =1.09

[a] between parenthesis, the relative amplitude of the fluorescence component.

Interaction of NBFT- CMβCyD with $[(CH_3)_8LZn]^{8+}$

UV-Vis absorption and fluorescence. UV-vis absorption titration in water has been performed keeping the $[(CH_3)_8LZn]^{8+}$ concentration (8 $\times 10^{-6}$ M) constant and varying the NBFT-CMβCyD

concentration (from 1×10^{-6} M to 2×10^{-5} M). In these conditions the initial monomer fraction of the octacation is 6 %. With increasing NBFT-CMβCyD concentration, the 655 nm/625 nm peak ratio decreases and an hypochromic effect is produced in the Soret absorption region of $[(CH_3)_8LZn]^{8+}$. Although the spectral variations are small, they are meaningful and clearly indicate that an interaction with the CyD derivative occurs and the $[(CH_3)_8LZn]^{8+}$ dimer is further stabilized in the bound state (Figure 2).

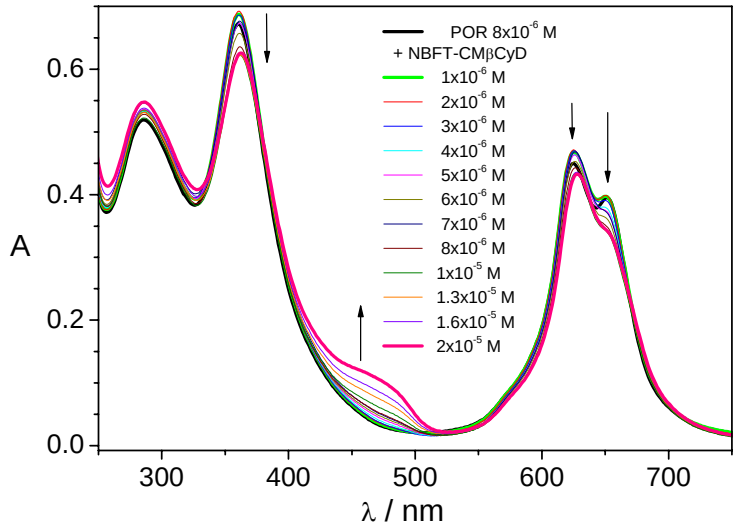

Figure 2. UV-visible absorption spectra of 8×10^{-6} M $[(CH_3)_8LZn]^{8+}$ (black) upon titration with NBFT-CMβCyD in the concentration range 1×10^{-6}M (green) - 2×10^{-5} M (pink); 1.0 cm cell, 22 °C.

The same mixtures were analyzed measuring the steady state fluorescence with selective excitation of $[(CH_3)_8LZn]^{8+}$ at 630 nm (Figure 3A), i.e. in a fairly isosbestic region (see Figure 2).[25] With increasing NBFT-CMβCyD concentrations the fluorescence intensity shows a progressive decrease. Considering the short lifetime of $[(CH_3)_8LZn]^{8+}$ we can exclude quenching due to partner diffusional encounter during the lifetime of the excited molecule and attribute the decreased fluorescence intensity to quenching in a ground state complex with the CyD host. The almost complete suppression of the $[(CH_3)_8LZn]^{8+}$ emission at the end of the titration is perfectly consistent

with a further shift of the monomer-dimer equilibrium toward the dimer, as inferred from the evolution of the absorption spectra.

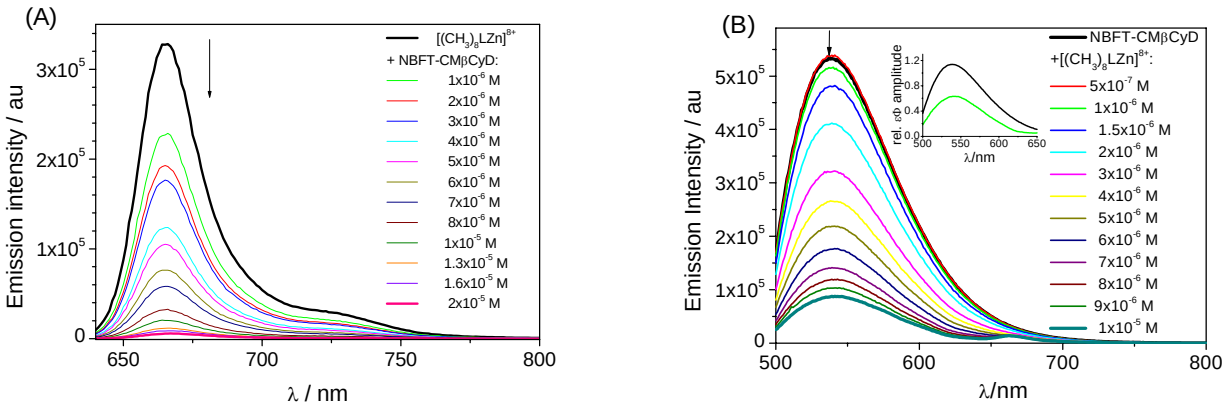

Figure 3. Emission spectra of (A) 8×10^{-6} M $[(CH_3)_8LZn]^{8+}$ upon titration with NBFT-CMβCyD in the concentration range 1×10^{-6}-2×10^{-5} M, λ_{exc} = 630 nm and (B) 5×10^{-6} M NBFT-CMβCyD upon titration with $[(CH_3)_8LZn]^{8+}$ in the concentration range 5×10^{-7}-1×10^{-5} M, λ_{exc} = 480 nm. T = 22 °C. Emission spectra are uncorrected. Inset (B): calculated fluorescence ε Φ amplitudes of the free host (black) and 2:2 complex (green).

Emission spectra in Figure 3B show a titration of 5×10^{-6} M NBFT-CMβCyD with $[(CH_3)_8LZn]^{8+}$ from 5×10^{-7} M to 1×10^{-5} M. Excitation at 480 nm was almost selective for the CyD host. Also the emission intensity of the NBFT chromophore decreased with the complexation progress. Diffusive quenching of the chromophore fluorescent state with lifetime 1.4 ns (see 3.3) is again excluded at the low $[(CH_3)_8LZn]^{8+}$ concentrations used in this experiment.

Global analysis of the NBFT-CMβCyD–$[(CH_3)_8LZn]^{8+}$ spectroscopic titrations. The set of spectra of Figure 2 were globally analysed with SPECFIT/32 (see ESI-3 for details) in the interval 550-700 nm, where $[(CH_3)_8LZn]^{8+}$ exclusively contributes to the absorption. The monomer-dimer equilibrium constant log (K_d/M^{-1}) = 7.1 and the absolute absorption spectra of the $[(CH_3)_8LZn]^{8+}$ monomer and dimer in water were taken from a previous study [11] and were kept fixed in the calculation. Formation of two complexes with 1:2 and 2:2 NBFT-CMβCyD: $[(CH_3)_8LZn]^{8+}$ stoichiometry was assessed with

$\log(K_{12}/M^{-2})$ = 13.4 ±0.5 and $\log(K_{22}/M^{-3})$ = 19.5 ±0.5 (DW 1.4). Figure 4A shows the absolute spectra of all the species in solution. The spectral features of the complexes clearly point to guest dimeric structure. The concentration profiles in Figure 4B show almost complete association of the $[(CH_3)_8LZn]^{8+}$ macrocycle to the CyD host in a predominant 2:2 stoichiometry complex. The quality of the agreement between calculated and experimental absorbances at representative wavelengths is reported in ESI-3-Figure S5.

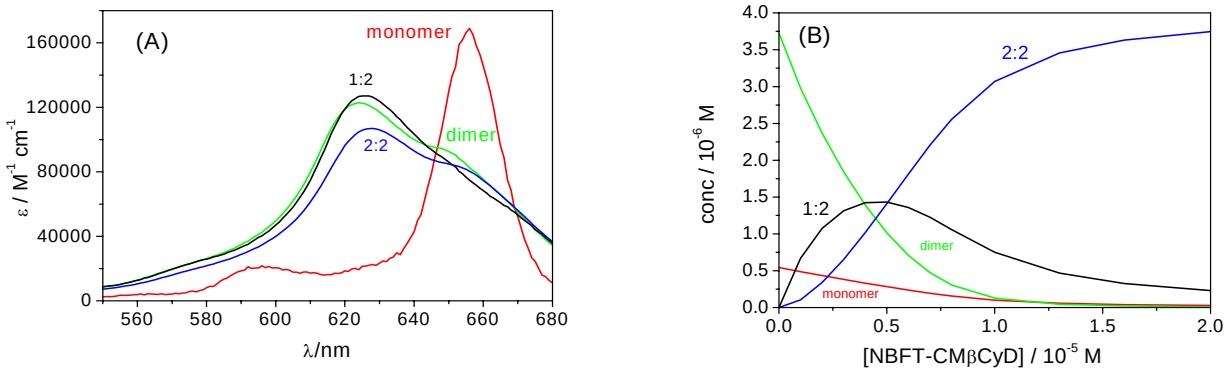

Figure 4. (A) Absolute absorption spectra of $[(CH_3)_8LZn]^{8+}$ monomer (red) [11] and $[(CH_3)_8LZn]^{8+}$ dimer (green) [11] and of the NBFT-CMβCyD: $[(CH_3)_8LZn]^{8+}$ 1:2 complex (black) and 2:2 complex (blue) for association constants $\log(K_{12}/M^{-2})$ = 13.4 and $\log(K_{22}/M^{-3})$ = 19.5; (B). Concentration profiles of all the species in solution (same color code).

Analysis of the fluorescence titration data in Figure 3A in the interval 640-800 nm was performed assuming that the only emitting species in the system is the $[(CH_3)_8LZn]^{8+}$ monomer (excitation at 630 nm is selective). Similar values of the association constants were obtained, $\log(K_{12}/M^{-2})$ = 14.3 ±0.3 and $\log(K_{22}/M^{-3})$ = 20.5 ±0.6 (DW 2.9). We also analyzed the data of Figure 3B, relevant to the emission intensity changes of NBFT-CMβCyD titrated with $[(CH_3)_8LZn]^{8+}$, in the region 500-640 nm, where the NBFT chromophore exclusively contributes. The solutions were optically thin (A at λ_{exc} < 0.1 over 1 cm path), so a linear dependence of fluorescence signal on the concentration is operative for all the species involved. The complexation model was essentially confirmed with $\log(K_{12}/M^{-2})$ = 14.2 ± 0.08 and $\log(K_{22}/M^{-3})$ = 20.5 fixed (DW

1.2). To obtain convergence it was necessary to assume that the emission of the NBFT chromophore is completely quenched in the 1:2 complex (i.e. this complex does not contribute to total intensity, see ESI-3) whereas emission survives in the 2:2 complex. According to the results of the calculations the molar emission contribution of the 2:2 complex is ca. 52 % that of the free host (from the integrated relative amplitudes represented in the inset of Figure 3B, each proportional to ε Φ with ε molar absorption coefficient for the excitation light). Considering that the ε value is about double in the 2:2 complex the average Φ is ca. 26 % that of the free NBFT-CMβCyD,. The emission decay measured with excitation 465 nm in a sample of NBFT-CMβCyD ca. 95% bound in the 2:2 complex (2×10^{-5} M NBFT-CMβCyD in presence of 8×10^{-6} M $[(CH_3)_8LZn]^{8+}$) is monoexponential with a lifetime of ~ 1.4 ns, the same as that of the free host. This fact indicates that, as expected, one of the two NBFT chromophores is strongly quenched whereas the other one is fairly unperturbed.

Interaction of pβCyD-Rh with $[(CH_3)_8LZn]^{8+}$

UV-vis absorption and fluorescence. The absorption spectrum of 3.25×10^{-6} M pβCyD-Rh in water reveals the occurrence of aggregation phenomena in the solution. Indeed, considering one rhodaminyl group every three oligomers we get a molar absorption coefficient $\varepsilon = 55383$ M^{-1} cm^{-1} at 557 nm for the rhodaminyl chromophore, which is quite low when compared to that of a free rhodamine species. This clearly indicates the oligomer is aggregated. The emission of the rhodaminyl moiety in pβCyD-Rh has a biexponential decay (Table 1) with lifetimes of 1.0 ns (60 %) and 2.6 ns (40 %). The two components are assigned either to monomeric and dimeric rhodaminyl species or two different environments for rhodaminyl groups in the oligomer frame.

Titration of 2×10^{-6} M $[(CH_3)_8LZn]^{8+}$ (14 % as monomer) in water with increasing amounts of pβCyD-Rh from 1.6×10^{-8} M to 8×10^{-7} M leads to changes in the absorption intensity and profile.

Two phases are observed: a progressive decrease of the $[(CH_3)_8LZn]^{8+}$ absorption bands (both the Soret and the Q-band system) up to 6.4×10^{-8} M oligomer; at higher oligomer concentrations a subsequent increase of the absorption, reaching a maximum at ca. 4.8×10^{-7} M (Figure 5); a progressive increase in the ratio of the $[(CH_3)_8LZn]^{8+}$ 625 nm peak to the 655 nm peak on increasing the oligomer concentration, pointing to an increase of the dimer fraction in the bound state.

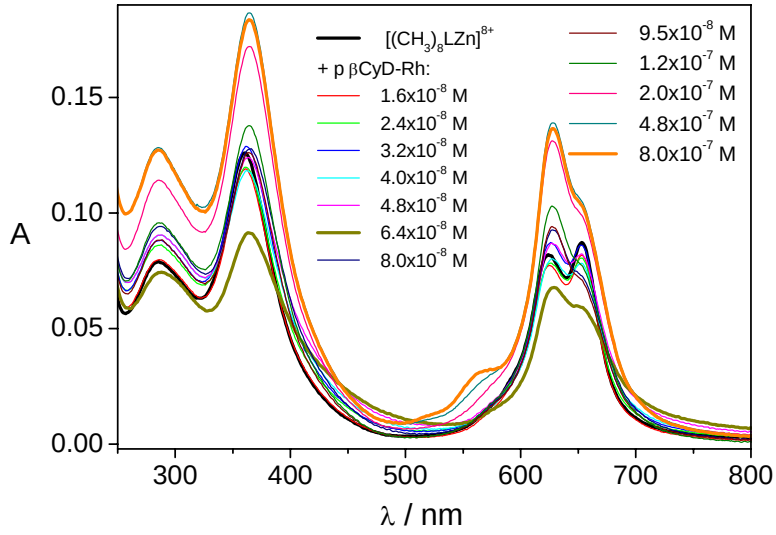

Figure 5. UV-visible absorption titration of 2×10^{-6} M $[(CH_3)_8LZn]^{8+}$ with pβCyD-Rh (from 1.6×10^{-8}M – 8×10^{-7} M) in water, cell path length 1 cm, 22 °C, water as reference.

The fluorescence spectra of the same mixtures with excitation at 630 nm, selective for $[(CH_3)_8LZn]^{8+}$, are shown in Figure 6. The emission of the $[(CH_3)_8LZn]^{8+}$ monomer is progressively quenched by the oligomer and has almost completely disappeared already at 8×10^{-8} M pβCyD-Rh. The emission of the rhodaminyl pendant on selective excitation at 530 nm is also quenched in part by $[(CH_3)_8LZn]^{8+}$. Figure 7A shows the effect of $[(CH_3)_8LZn]^{8+}$ on pβCyD-Rh at various concentrations. The quenching shows two phases, reasonably assigned to the progress of two different complexation steps (Figure 7B).

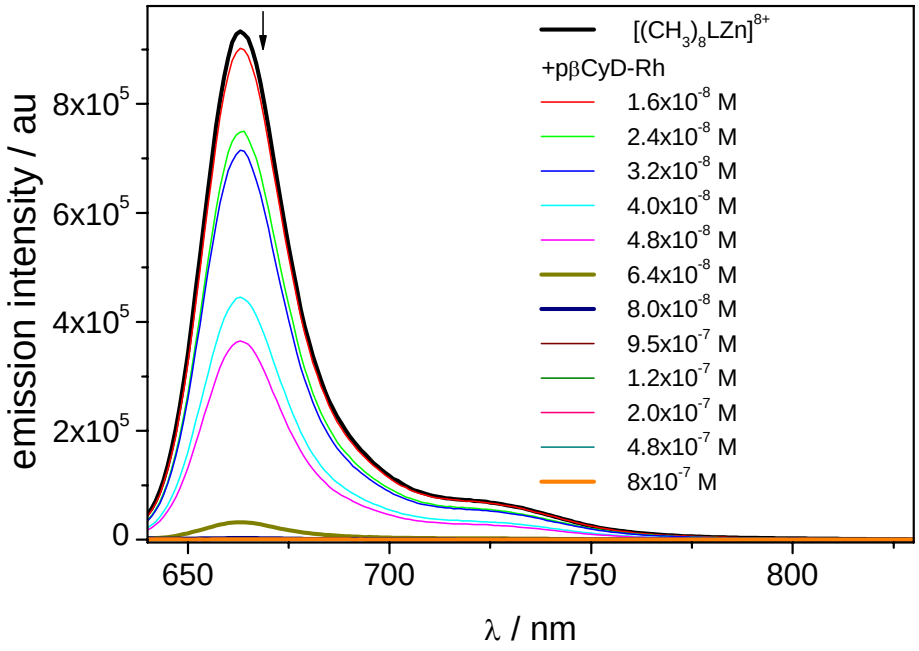

Figure 6. Emission spectra of 2×10^{-6} M $[(CH_3)_8LZn]^{8+}$ upon titration with pβCyD-Rh (from 1.6×10^{-8} M to 8×10^{-7} M) in water, λ_{exc} = 630 nm and T =22 °C. Spectra are uncorrected.

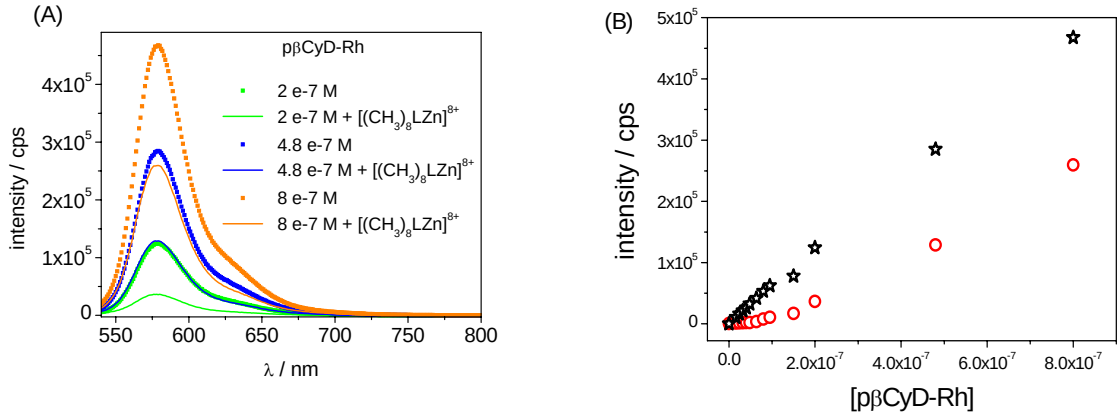

Figure 7. (A) Quenching of the fluorescence intensity of pβCyD-Rh at various concentrations in water by 2×10^{-6} M $[(CH_3)_8LZn]^{8+}$, λ_{exc} = 530 nm, T = 22 °C. Emission spectra are uncorrected. (B) Dependence of the rhodaminyl fluorescence intensity on the concentration of pβCyD-Rh alone (black) and in presence of 2×10^{-6} M $[(CH_3)_8LZn]^{8+}$ (red).

Global analysis of the pβCyD-Rh̃[(CH$_3$)$_8$LZn]$^{8+}$ spectroscopic titrations. The best equilibrium model and the association constants were determined by means of global analysis of the absorption data of Figure 5 in the interval 550-700 nm, expressing the host concentration in terms of CMβCyD units. The monomer-dimer equilibrium constant in water (log (K_d/M^{-1}) = 7.1) and the absorption spectra of

the $[(CH_3)_8LZn]^{8+}$ monomer and dimer, [11] were fixed. The absorption spectrum of the rhodaminyl moiety was also fixed, averaged on the concentration of CMβCyD units (we recall that the CMβCyD content of the oligomer is 60 % and on average every third oligomer molecule contains one rhodaminyl group). Formation of two complexes with 1:2 and 2:2 CMβCyD:$[(CH_3)_8LZn]^{8+}$ stoichiometry and $\log(K_{12}/M^{-2}) = 20.7 \pm 0.2$ and $\log(K_{22}/M^{-3}) \approx 27$ was found to reasonably reproduce the absorption data. The 2:2 association constant needs to be fixed in the calculation, but only $pK_{22} \approx 27$ allows convergence. Figure 8A and 8B show the absolute spectra and the concentration profiles of all the species.

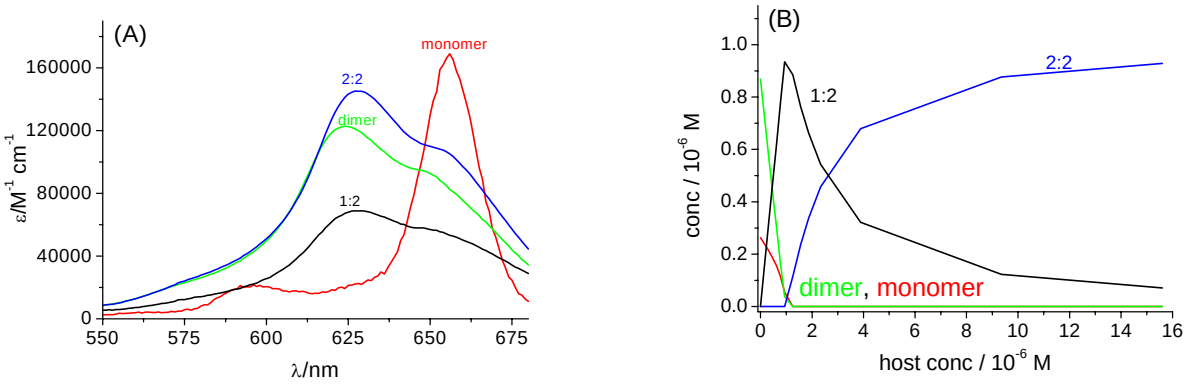

Figure 8. (A) Absolute spectra of $[(CH_3)_8LZn]^{8+}$ monomer (red) and dimer (green), [11] and CMβCyD: $[(CH_3)_8LZn]^{8+}$ 1:2 (black) and 2:2 (blue) complexes in water. See text for the association constants. (B). Concentration profiles of all the species in solution.

Global analysis of the data in Figure 6 assuming the only emitting species is the $[(CH_3)_8LZn]^{8+}$ monomer, confirmed the complexation model with 1:2 and 2:2 CMβCyD:$[(CH_3)_8LZn]^{8+}$ stoichiometry and the association constants as $\log (K_{12}/M^{-2}) = 18.1 \pm 1.7$ and $\log (K_{22}/M^{-3}) \approx 26.7 \pm 2$ (DW 2.3). As noticed with the NBFT-CMβCyD host, the absorption spectra of the complexes in Figure 8A clearly show the dimeric structure for $[(CH_3)_8LZn]^{8+}$ in the bound state. Again, almost complete association of dimeric pyrazinoporphyrazine takes place with either one or two negatively charged CMβCyD units of pβCyD-Rh.

4. Conclusions

Combination of spectroscopic titrations and global analysis of multiwavelength data has provided a reliable description of the interaction of a selfassociating porphyrazine macrocycle with CyD systems of both monomeric and polymeric structure. This approach, we believe, has a good potential as analytical and characterization tool for the investigation and optimization of new third generation macrocyclic photosensitizers and in general of host:guest systems involving complex equilibria.

The $[(CH_3)_8LZn]^{8+}$ guest binds almost exclusively as dimer to both NBFT-CMβCyD and pβCyD-Rh in water. CyD:guest complexes with 1:2 and 2:2 stoichiometry are indeed formed with both host systems. The pyrazinoporphyrazine macrocycle is not believed to penetrate deeply into the CyD cavity, because of its large size and peripheral positive charges. Stabilization of the $[(CH_3)_8LZn]^{8+}$ dimer by the CyD units is reasonably attributed to the interaction with the negative carboxylate groups, able to determine complete conversion of the $[(CH_3)_8LZn]^{8+}$ free monomer fraction to the dimer state in the bound condition. Indeed the width of the macrocycle and the diameter of the cyclodextrin secondary face are very similar to each other. It can therefore be hypothesized that the distribution of the positive charges in the two $[(CH_3)_8LZn]^{8+}$ units of the dimer and of the carboxylate negative charges of the CMβCyD units allow establishment of multiple host:guest ionic bonds in the complexes, strongly favouring 1:2 and 2:2 structures. Because the $[(CH_3)_8LZn]^{8+}$ dimer is negligibly fluorescent, host-induced dimerization is the most likely mechanism at the basis of the $[(CH_3)_8LZn]^{8+}$ fluorescence quenching in the presence of either NBFT-CMβCyD or the pβCyD-Rh oligomer. At low CMβCyD concentrations one unit binds to the $[(CH_3)_8LZn]^{8+}$ in dimeric form. At higher concentrations one more CyD unit adds, contributing to the establishment of a final population with the 2:2 complex as largely predominant species.

Both 1:2 and 2:2 complexes with the CMβCyD units of the pβCyD-Rh oligomer have average stability constants by 6-7 orders of magnitude larger than those with the monomeric CMβCyD moiety of the NBFT labelled derivative. The different chemical nature of the fluorescent label is not believed to play a key role. Rather, according to previous findings relevant to the binding affinities of monomeric and polymeric CyD hosts vs. the same guest,[20] the high local CyD concentration and the 3D spatial organization of the oligomer are the most likely reasons for such a large increase in the $[(CH_3)_8LZn]^{8+}$ binding constants. This is a positive outcome for the application of similar CyD oligomers as carriers of highly charged singlet oxygen photosensitizers. Indeed from the biological point of view, e.g. for cell penetration, we reasonably expect a more favourable behaviour of the oligomer complexed $[(CH_3)_8LZn]^{8+}$, partly neutralized, compared to the isolated octacation. Unfortunately, the carrier is not capable of disrupting the $[(CH_3)_8LZn]^{8+}$ dimer in aqueous environment, which could represent a drawback in the frame of singlet oxygen sensitization. This behaviour differs from that of other CyD derivatives with polymeric structure, either neutral or negatively charged, which are able to contrast, for example, the selfassociation of doxorubicin in neutral buffer.[19, 20] However we envisage that biological actors can promote monomerization of $[(CH_3)_8LZn]^{8+}$ once the photosensitizer has been vehicled inside the cell. Indeed, it is worth recalling that the $[(CH_3)_8LZn]^{8+}$ dimer is partly disrupted upon binding to G4-DNA[10]

Acknowledgements

We thank Professor Claudio Ercolani (University of Rome "La Sapienza") for helpful discussions and the FP7 PEOPLE-ITN project n. 237962-CYCLON for the funding of the research. We also thank CNR project NANOMAX for financial support.

References

1. P. A. Stuzhin and C. Ercolani, in *The Porphyrin Handbook; Phthalocyanines: Synthesis*, eds. K. M. Kadish, K. M. Smith and R. Guilard, Academic Press, New York, 2003, vol. 15 pp.

263-364; M. S. Rodriguez-Morgade and P. A. Stuzhin, *J. Porphyr. Phthalocyanines*, 2004, **8**, 1129-1165; T. Fukuda and N. Kobayashi, *Dalton Transactions*, 2008, 4685-4704.

2. M. J. Fuchter, C. Zhong, H. Zong, B. M. Hoffman and A. G. M. Barrett, *Aust. J. Chem.*, 2008, **61**, 235-255.
3. E. J. Baerends, G. Ricciardi, A. Rosa and S. J. A. van Gisbergen, *Coord. Chem. Rev.*, 2002, **230**, 5-27; M. P. Donzello, D. Dini, G. D'Arcangelo, C. Ercolani, R. Q. Zhan, Z. P. Ou, P. A. Stuzhin and K. M. Kadish, *J. Am. Chem. Soc.*, 2003, **125**, 14190-14204; M. P. Donzello, R. Agostinetto, S. S. Ivanova, M. Fujimori, Y. Suzuki, H. Yoshikawa, J. Shen, K. Awaga, C. Ercolani, K. M. Kadish and P. A. Stuzhin, *Inorg. Chem.*, 2005, **44**, 8539-8551.
4. M. P. Donzello, Z. P. Ou, D. Dini, M. Meneghetti, C. Ercolani and K. M. Kadish, *Inorg. Chem.*, 2004, **43**, 8637-8648; M. P. Donzello, Z. P. Ou, F. Monacelli, G. Ricciardi, C. Rizzoli, C. Ercolani and K. M. Kadish, *Inorg. Chem.*, 2004, **43**, 8626-8636.
5. C. Bergami, M. P. Donzello, C. Ercolani, F. Monacelli, K. M. Kadish and C. Rizzoli, *Inorg. Chem.*, 2005, **44**, 9852-9861.
6. C. Bergami, M. P. Donzello, F. Monacelli, C. Ercolani and K. M. Kadish, *Inorg. Chem.*, 2005, **44**, 9862-9873.
7. M. P. Donzello, D. Vittori, E. Viola, I. Manet, L. Mannina, L. Cellai, S. Monti and C. Ercolani, *Inorg. Chem.*, 2011, **50**, 7391-7402.
8. M. P. Donzello, E. Viola, M. Giustini, C. Ercolani and F. Monacelli, *Dalton Transactions*, 2012, **41**, 6112-6121.
9. I. Manet, F. Manoli, M. P. Donzello, C. Ercolani, D. Vittori, L. Cellai, A. Masi and S. Monti, *Inorg. Chem.*, 2011, **50**, 7403-7411.
10. I. Manet, F. Manoli, M. P. Donzello, E. Viola, G. Andreano, A. Masi, L. Cellai and S. Monti, *Org. Biomol. Chem.*, 2011, **9**, 684-688.
11. I. Manet, F. Manoli, M. P. Donzello, E. Viola, A. Masi, G. Andreano, G. Ricciardi, A. Rosa, L. Cellai, C. Ercolani and S. Monti, *Inorg. Chem.*, 2013, **52**, 321-328.
12. T. J. Jensen, M. G. a. H. Vicente, R. Luguya, J. Norton, F. R. Fronczek and K. M. Smith, *J. Photochem. Photobiol. B: Biology*, 2010, **100**, 100-111.
13. D. Kessel, R. Luguya and M. G. a. H. Vicente, *Photochem. Photobiol.*, 2003, **78**, 431-435.
14. A. E. O'Connor, W. M. Gallagher and A. T. Byrne, *Photochem. Photobiol.*, 2009, **85**, 1053-1074.
15. Y.-Y. Huang, P. Mroz, T. Zhiyentayev, S. K. Sharma, T. Balasubramanian, C. RuzieÌ , M. Krayer, D. Fan, K. E. Borbas, E. Yang, H. L. Kee, C. Kirmaier, J. R. Diers, D. F. Bocian, D. Holten, J. S. Lindsey and M. R. Hamblin, *J. Med. Chem.*, 2010, **53**, 4018-4027.
16. M. E. Davis and M. E. Brewster, *Nat Rev Drug Discov*, 2004, **3**, 1023-1035; T. Loftsson and M. E. Brewster, *J. Pharm. Sci.*, 1996, **85**, 1017-1025; M. E. Brewster and T. Loftsson, *Adv. Drug Deliv. Rev.*, 2007, **59**, 645-666; F. van de Manakker, T. Vermonden, C. F. van Nostrum and W. E. Hennink, *Biomacromolecules*, 2009, **10**, 3157-3175; A. Ueno, *Supramolecular Science*, 1996, **3**, 31-36.
17. A. Mazzaglia, N. Micali, L. M. Scolaro, M. T. Sciortino, S. Sortino and V. Villari, *J. Porphyr. Phthalocyanines*, 2010, **14**, 661-677; N. Kandoth, E. Vittorino, M. T. Sciortino, T. Parisi, I. Colao, A. Mazzaglia and S. Sortino, *Chem.-Eur. J.*, 2012, **18**, 1684-1690.
18. E. Renard, A. Deratani, G. Volet and B. Sebille, *Eur. Polym. J.*, 1997, **33**, 49-57; R. Gref, C. Amiel, K. Molinard, S. Daoud-Mahammed, B. Sebille, B. Gillet, J. C. Beloeil, C. Ringard, V. Rosilio, J. Poupaert and P. Couvreur, *J. Control. Release*, 2006, **111**, 316-324; S. Daoud-Mahammed, P. Couvreur, K. Bouchemal, M. Cheron, G. Lebas, C. Amiel and R. Gref, *Biomacromolecules*, 2009, **10**, 547-554.

19. R. Anand, F. Manoli, I. Manet, S. Daoud-Mahammed, V. Agostoni, R. Gref and S. Monti, *Photochem. Photobiol. Sci.*, 2012, **11**, 1285-1292.
20. R. Anand, M. Malanga, I. Manet, F. Manoli, K. Tuza, A. Aykaç, L. C, E. Fenyvesi, A. Vargas-Berenguel, R. Gref and S. Monti, *Photochem. Photobiol. Sci.* 2013, **12**, 1841-1854.
21. A. Fraix, N. Kandoth, I. Manet, V. Cardile, A. C. E. Graziano, R. Gref and S. Sortino, *Chem. Commun.*, 2013, **49**, 4459-4461; E. Deniz, N. Kandoth, A. Fraix, V. Cardile, A. C. E. Graziano, D. Lo Furno, R. Gref, F. M. Raymo and S. Sortino, *Chem.-Eur. J.*, 2012, **18**, 15782-15787.
22. Y. F. He, P. Fu, X. H. Shen and H. C. Gao, *Micron*, 2008, **39**, 495-516; R. N. Dsouza, U. Pischel and W. M. Nau, *Chem. Rev.*, 2011, **111**, 7941-7980.
23. I. Puskas, A. Szemjonov, E. Fenyvesi, M. Malanga and L. Szente, *Carbohydr. Polym.*, 2013, **94**, 124-128.
24. N. W. McGill and S. J. Williams, *J. Org. Chem.*, 2009, **74**, 9388-9398.
25. The absorbance of the [(CH3)8LZn]8+ solution at 630 nm in the experiment of Figure 3A was ca. 0.4 over 1 cm. This high value did not introduce error, because it is kept fairly constant in the course of the titration (see Figure 2).

Graphical Abstract

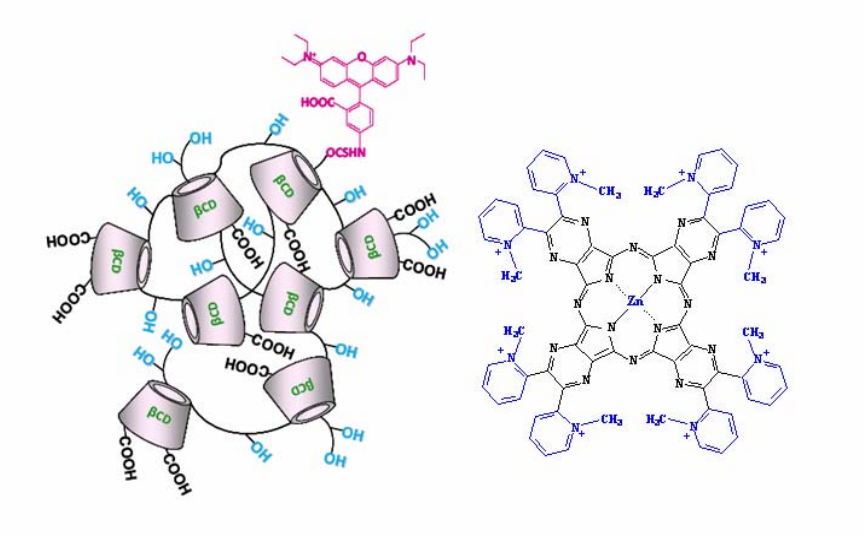

New negatively charged, fluorescent cyclodextrin oligomers form highly stable complexes with a water soluble, octacationic porphyrazine photosensitizer in dimeric form.

ELECTRONIC SUPPLEMENTARY INFORMATION

Fluorescent cyclodextrin carriers for a water soluble Zn^{II} pyrazinoporphyrazine octacation with photosensitizer potential

R. Anand,[1] F. Manoli,[1] I. Manet,[1] M. P. Donzello,[2] E. Viola,[2] M. Malanga,[3] L. Jicsinszky,[3] E. Fenyvesi,[3] S. Monti[1]*

[1] Istituto per la Sintesi Organica e la Fotoreattività, Consiglio Nazionale delle Ricerche , via P. Gobetti 101, I-40129 Bologna, Italy
[2] Dipartimento di Chimica, Università degli Studi di Roma "La Sapienza", P.le A. Moro 5, I-00185 Roma, Italy
[3] CycloLab, Cyclodextrin R&D Ltd., Illatos út 7, H-1097 Budapest, Hungary

ESI-1. SPECTROSCOPIC DATA ON SYNTHESIZED MATERIALS

ESI-2. SELF-AGGREGATION OF $[(CH_3)_8LZn]^{8+}$

ESI-3 GLOBAL ANALYSIS OF EQUILIBRIUM SPECTROSCOPIC DATA

ESI-1. SPECTROSCOPIC DATA ON SYNTHESIZED MATERIALS

IR

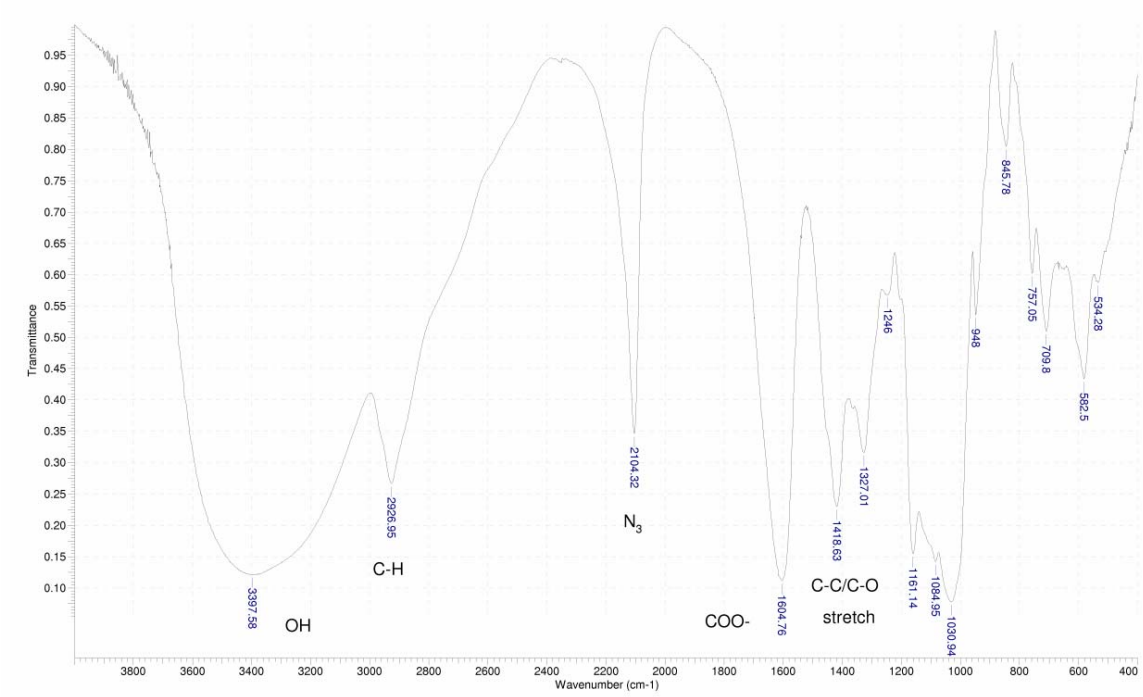

^{1}H-NMR

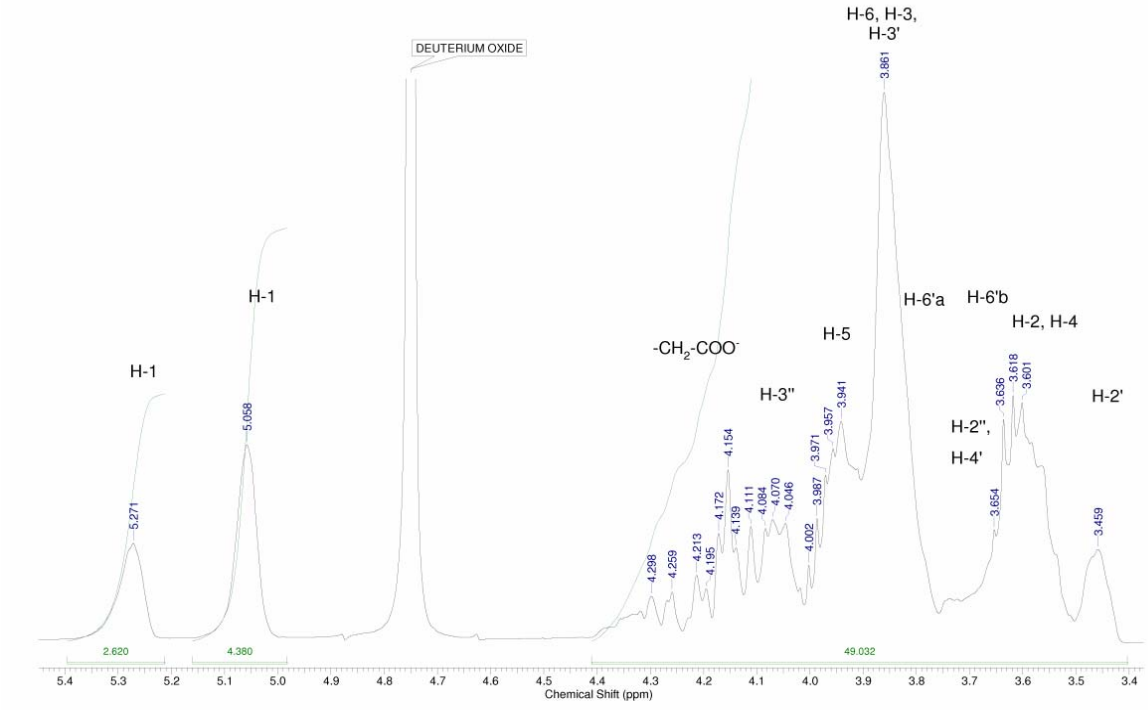

^{13}C-NMR

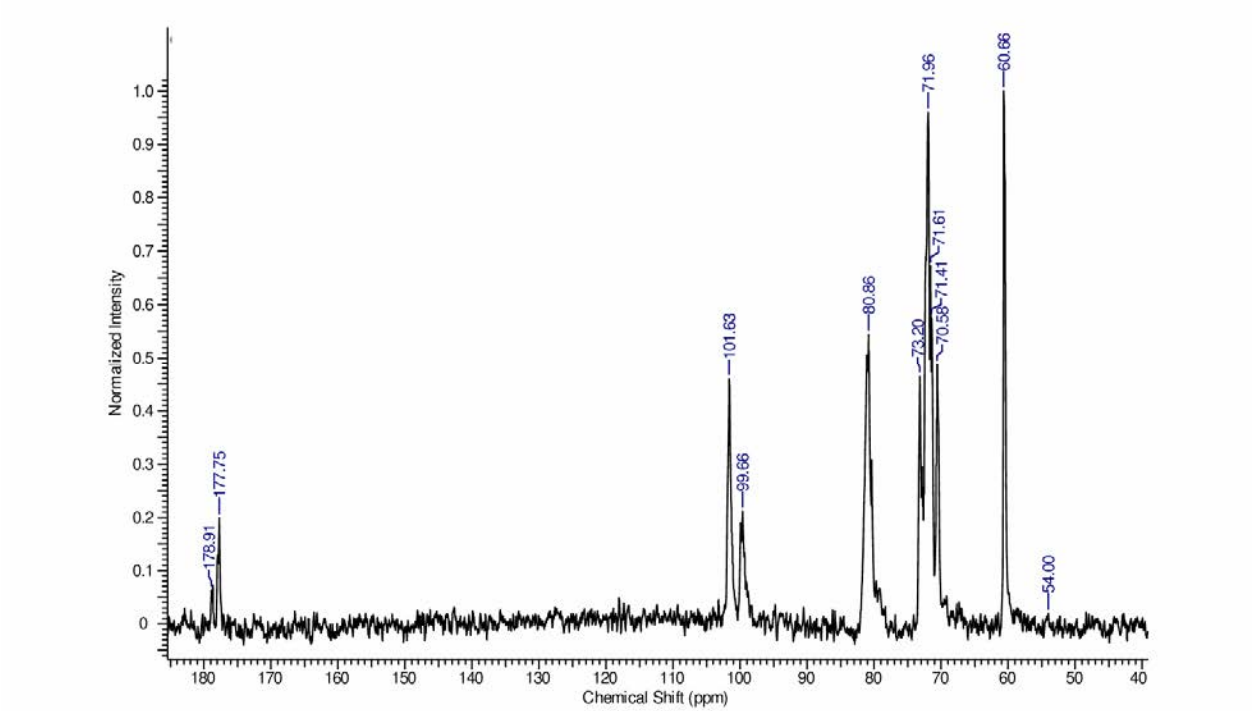

HSQC- DEPT

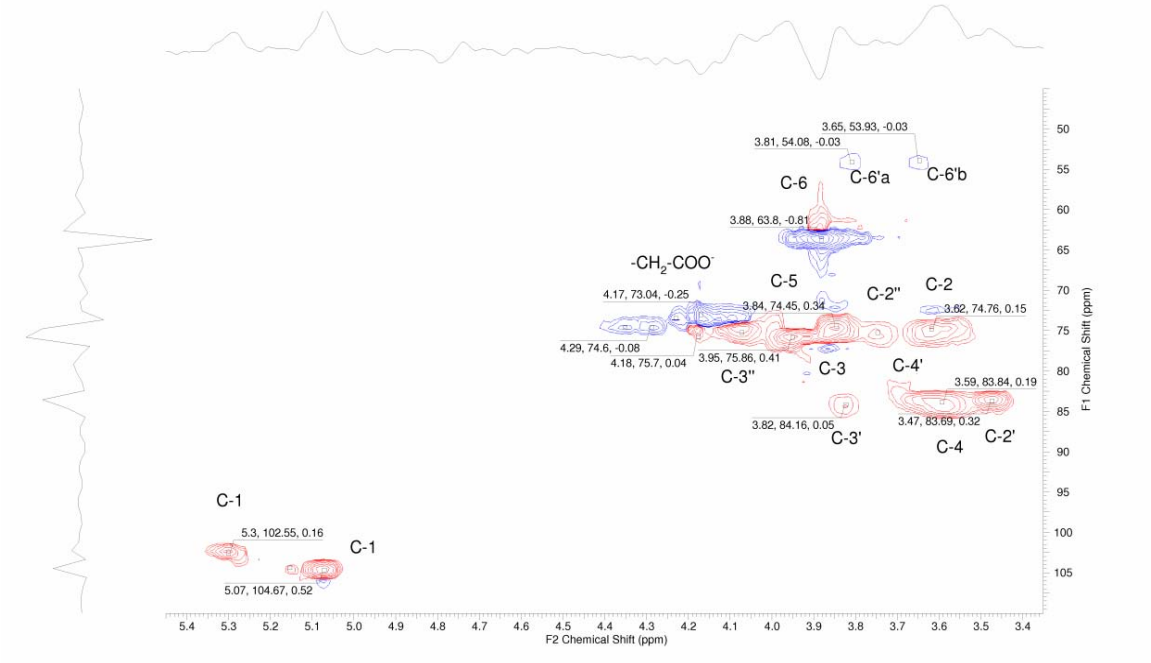

Figure S1. IR, ^{1}H-NMR, ^{13}C-NMR and HSQC-DEPT of 6-monodeoxy-6-monoazido-carboxy-methyl-β-CyD sodium salt.

^{1}H-NMR

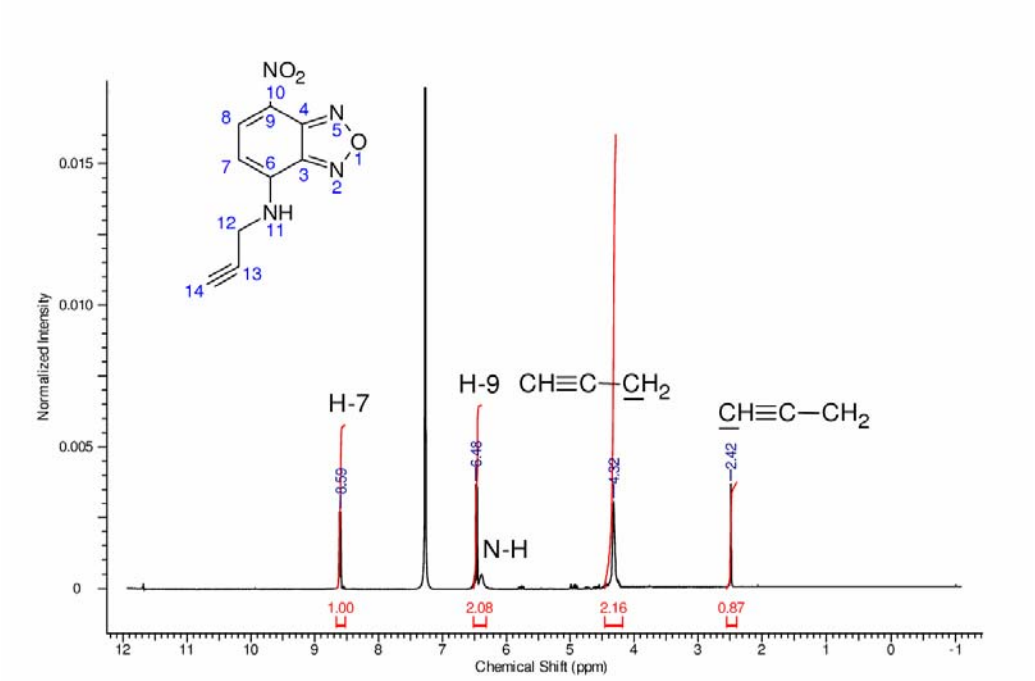

ESI-MS

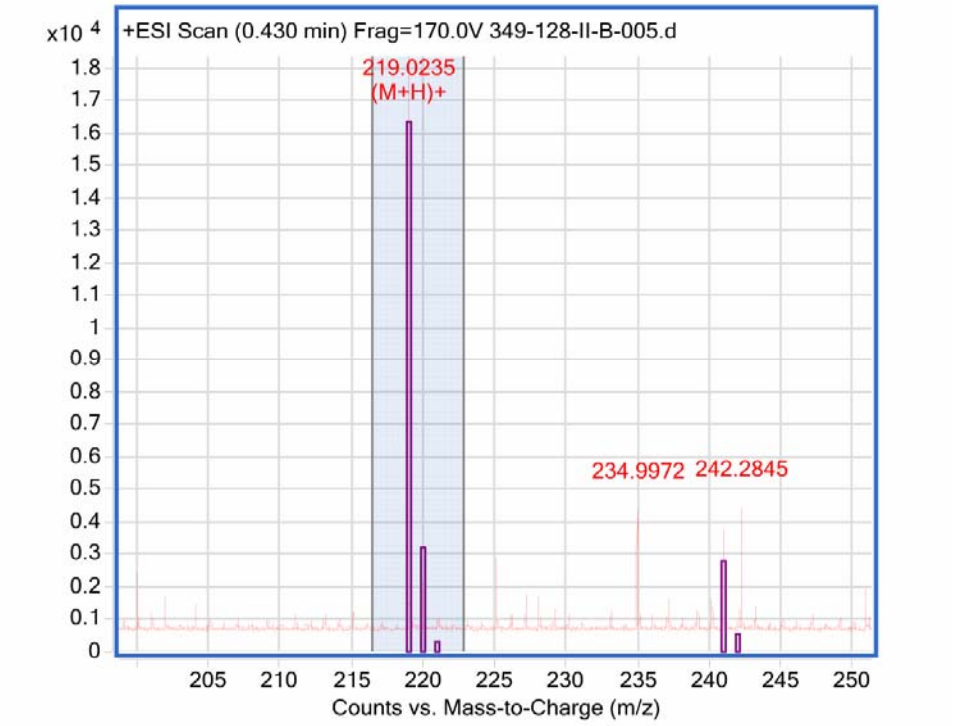

Figure S2: ^{1}H-NMR and ESI-MS of mono-4-(N-propargyl)-7-nitrobenzofuran.

IR

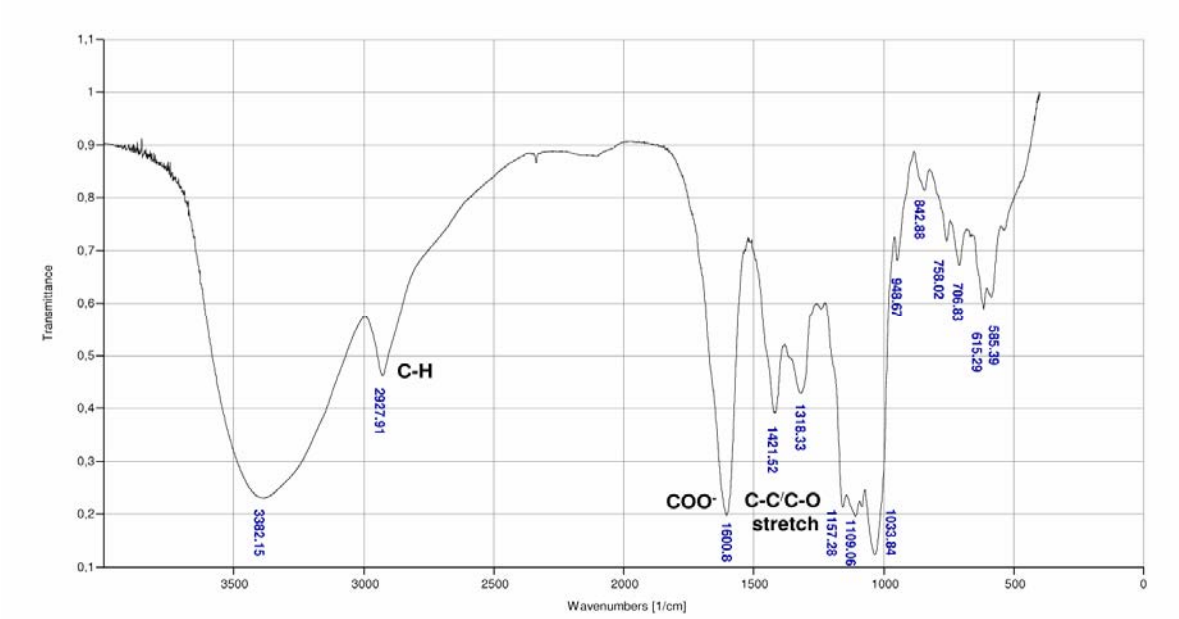

^{1}H-NMR

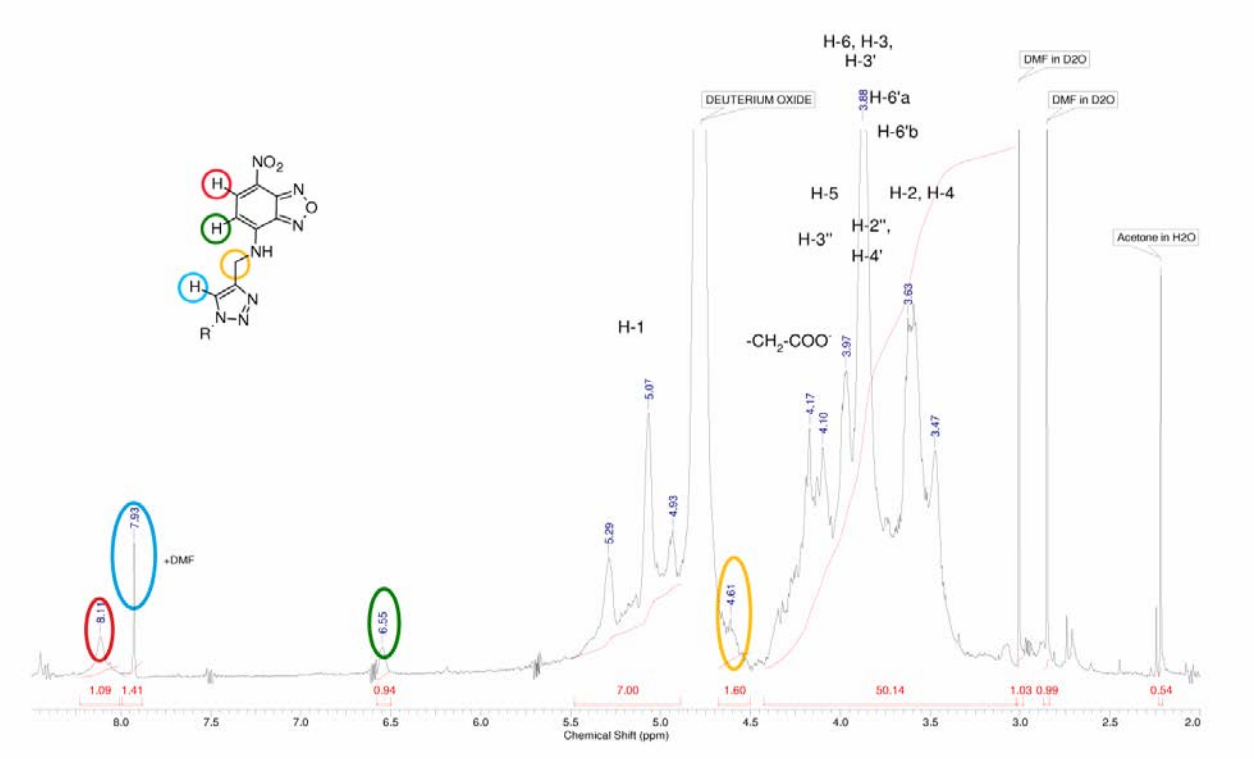

^{13}C-NMR

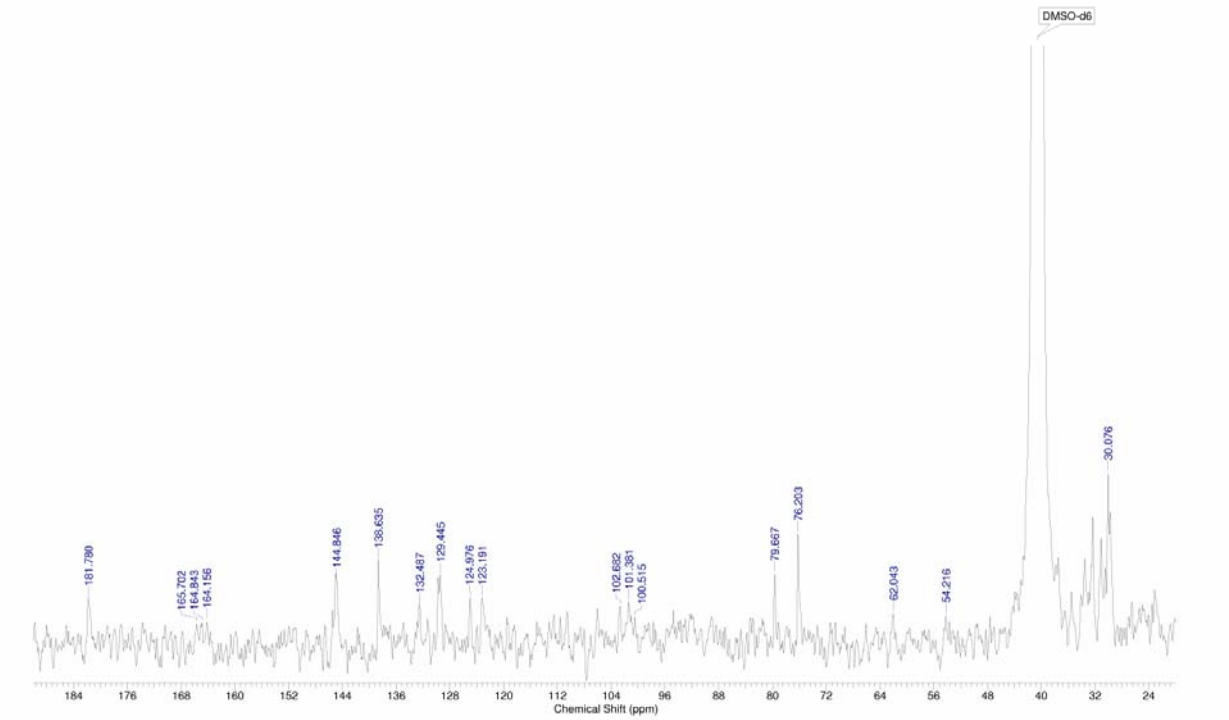

HSQC-DEPT

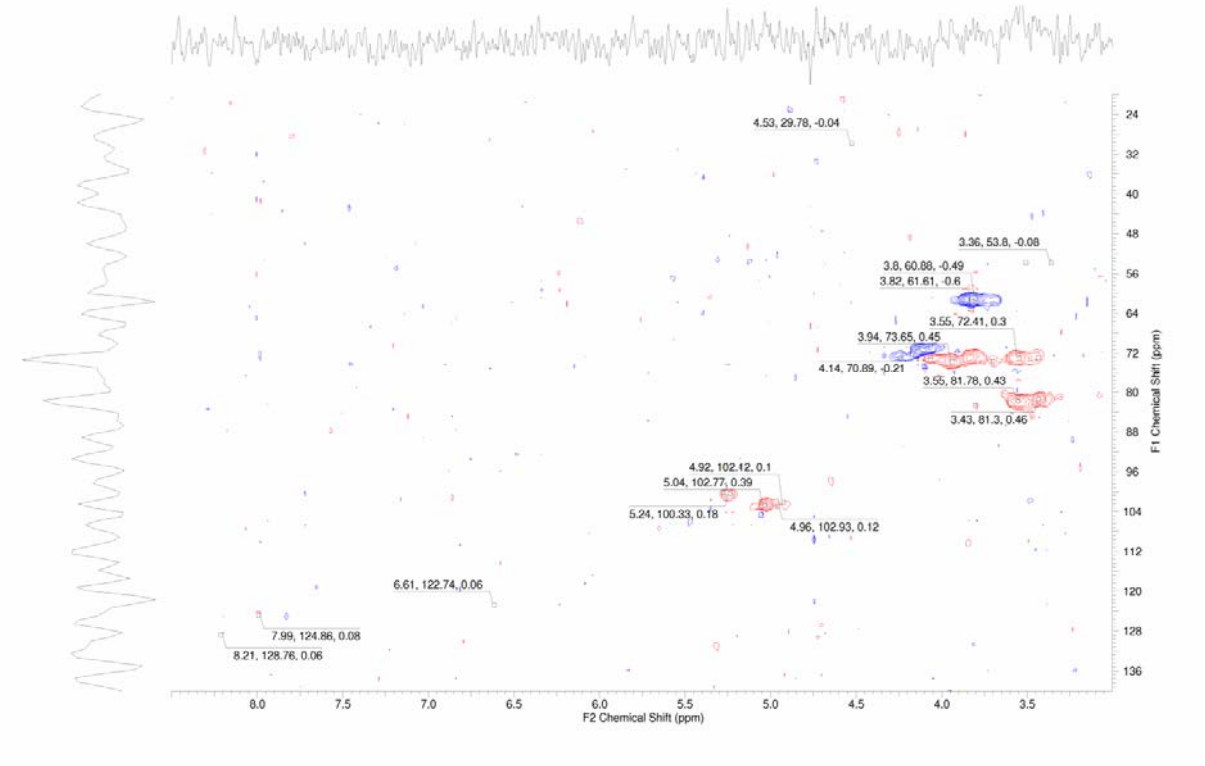

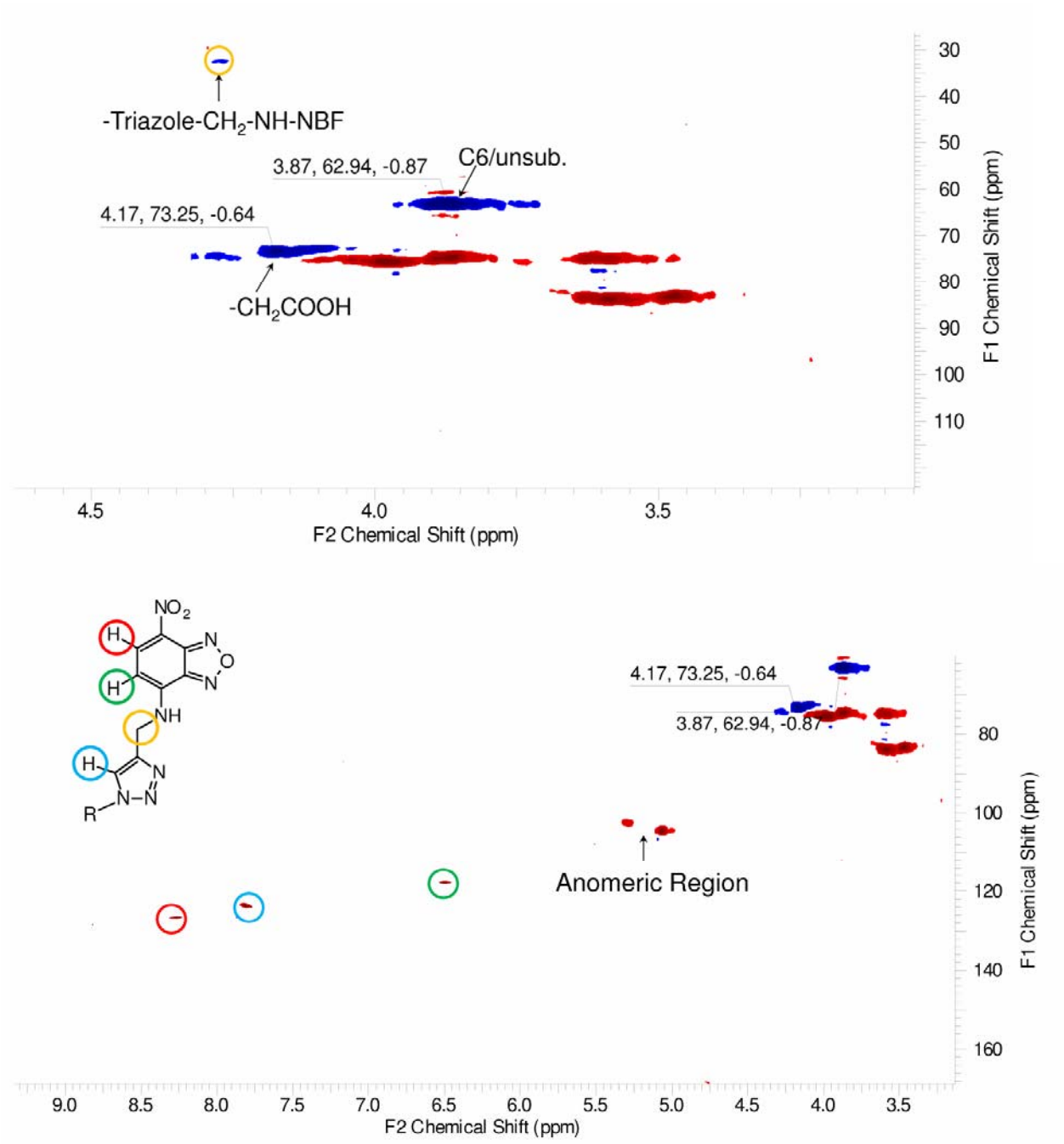

Figure S3 IR, ^{1}NMR, ^{13}C-NMR and HSQC-DEPT spectra of nitrobenzofurazan-NH-triazolyl-carboxymethyl-β-CyD..

ESI-2. SELF-AGGREGATION OF $[(CH_3)_8LZn]^{8+}$

The UV-visible absorption spectrum of $[(CH_3)_8LZn]^{8+}$ in water (Figure S4) is characterized by a Q band system with two maxima of comparable intensity at ca. 625 and 655 nm, attributed to the dimer and monomer, respectively, in equilibrium with log (K_d/M^{-1}) = 7.1. [1,2] The broad envelope in the Soret region at 300-400 nm is composed of π, π* transitions. The spectrum of the purely monomeric $[(CH_3)_8LZn]^{8+}$ was obtained in the presence of sodium dodecylsulfate (SDS) micelles.[2] It exhibits a dominating peak at ca. 660 nm, thanks to association of the octacationic macrocycle to the negatively charged micelle surface.

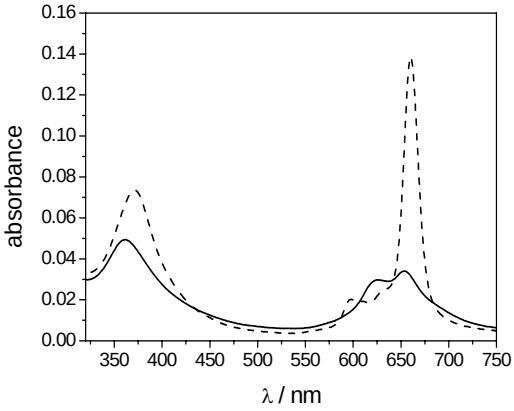

Figure S4. Absorption spectra of 1×10^{-6} M solution of $[(CH_3)_8LZn]^{8+}$ in water (solid line) and in water with 20 mM SDS (dashed line); cell path length 1.0 cm, 22 °C.

ESI-3.GLOBAL ANALYSIS OF EQUILIBRIUM SPECTROSCOPIC DATA

The receptor-ligand complexation equilibria were investigated by performing spectroscopic titrations. The best complexation model and the association constants were determined by multivariate global analysis of multiwavelength data from a series of spectra (UV-vis absorption, circular dichroism or fluorescence) corresponding to different mixtures, using the commercial

SPECFIT/32 (v.3.0.40, TgK Scientific) program.[3,4] Multiwavelength spectroscopic data sets (absorbances, ellipticities or fluorescence intensities) are arranged in matrix form **Y**, where a number Nw of wavelengths and a number Nm of corresponding measured spectroscopic signals are ordered in columns, whereas ligand and receptor concentrations are inserted in rows. Thus each element of the data matrix Y_{ij} corresponds to a wavelength j and an experimental quantity (absorbance, ellipticity or fluorescence intensity) for a given couple of concentrations i of ligand and receptor (typically in our experiments one of them is kept constant). A least square best estimator **Y'** of the original data **Y** is reconstructed as the eigenvector representation **Y'** = **U×S×V**, where **S** is a vector that contains the relative weights of the significant eigenvectors (Ne, number of significant eigenvectors), **U** is a matrix (Nm×Ne) of concentration eigenvectors ($U^T \times U=1$, orthonormal) and **V** (Ne×Nw) is a matrix of spectroscopic eigenvectors ($V \times V^T$, orthonormal). This **Y'** matrix contains less noise than **Y** because the SVD procedure can factor random noise from the principal components. This reconstructed data matrix **Y'** is utilized in the global fitting instead of the original data matrix **Y**. Complexation equilibria are solved assuming a complexation model (i.e. contemporary presence of a number of complexes of given stoichiometries in equilibrium with free species in solution) and optimizing the numeric combination of all the spectroscopic contributions ("colored" species) to best reproduce the **Y'** signals. The analysis relies mainly to absorption data, but also CD and fluorescence data may be analysed, in the latter case provided they are relevant to optically thin samples (linear dependence of fluorescence signal on concentration for all the species involved). Given the direct linearity between experimental signal and concentration and the relation that must exist between the concentrations of the various species in the postulated simultaneous equilibria, the program calculates the conditional association constants and the spectra of the complexes based on a non linear least square fit, using the Levenberg-Marquardt algorithm, to best reproduce the experimental data for all the explored wavelengths and ligand-receptor concentration

couples. The quality of the fits was evaluated on the basis of their Durbin-Watson (DW) factor and the relative error of fit. The DW test is very useful to check for the presence of auto-correlation in the residuals. This method is recommended for systematic misfit errors that can arise in titration experiments. It examines the tendency of successive residual errors to be correlated. The Durbin-Watson statistics ranges from 0.0 to 4.0, with an optimal mid-point value of 2.0 for uncorrelated residuals (i.e. no systematic misfit). In contrast to the χ^2 (Chi-squared) statistics, which requires the noise in the experimental data is random and normally distributed, the DW factor is meaningful even when the noise level in the data set is low. Since the factorized data usually have a significantly lower noise level than the original data, DW test is ideal for the present type of data.

We applied this method to analyze UV-vis absorption, and FL titration experiments. Below, as an example, we describe the analysis of the UV-visible absorption changes of 8×10^{-6} M $[(CH_3)_8LZn]^{8+}$ upon titration with NBFT-CMβCyD from 1×10^{-6} M to 2×10^{-5} M at 22 °C (data of Figure 2 in the main text).

[FACTOR ANALYSIS]

Tolerance = 1.000E-09

Max.Factors = 10

Num.Factors = 7

Significant = 4

Eigen Noise = 2.586E-04

Exp't Noise = 2.586E-04

Eigenvalue Square Sum Residual Prediction

1 1.258E+02 5.952E-02 5.913E-03 Data Vector

2 4.991E-02 9.608E-03 2.377E-03 Data Vector

3 9.188E-03 4.201E-04 4.971E-04 Data Vector

4 3.066E-04 1.136E-04 2.586E-04 Data Vector

5 3.226E-05 8.133E-05 2.189E-04 Probably Noise

6 1.685E-05 6.448E-05 1.949E-04 Probably Noise

7 1.396E-05 5.053E-05 1.726E-04 Probably Noise

[SPECIES]	[COLORED]	[FIXED]	[SPECTRUM]
1 0 0	False	False	receptor
0 1 0	True	True Monomer.FIX	ligand
0 2 0	True	True Dimer.FIX	ligand
1 2 0	True	False	complex
2 2 0	True	False	complex

[SPECIES]	[FIXED]	[PARAMETER]	[ERROR]
1 0 0	True	0.00000E+00 +/-	0.00000E+00
0 1 0	True	0.00000E+00 +/-	0.00000E+00
0 2 0	True	7.10000E+00 +/-	0.00000E+00
1 2 0	False	1.33762E+01 +/-	5.26377E-01
2 2 0	False	1.94962E+01 +/-	4.57734E-01

[CONVERGENCE]

Iterations = 5

Convergence Limit = 1.000E-04

Convergence Found = 3.059E-05

Marquardt Parameter = 0.0

Sum(Y-y)^2 Residuals = 4.37462E-02

Std. Deviation of Fit(Y) = 5.06980E-03

[STATISTICS]

Experimental Noise = 2.586E-04

Relative Error Of Fit = 2.5789%

Durbin-Watson Factor = 1.3667

Goodness Of Fit, Chi^2 = 3.844E+02

Durbin-Watson Factor (raw data) = 1.3682

Goodness Of Fit, Chi^2 (raw data) = None

[COVARIANCE]

5.571E+00 3.752E+00

3.752E+00 3.493E+00

[CORRELATION]

1.000E+00 8.504E-01

8.504E-01 1.000E+00

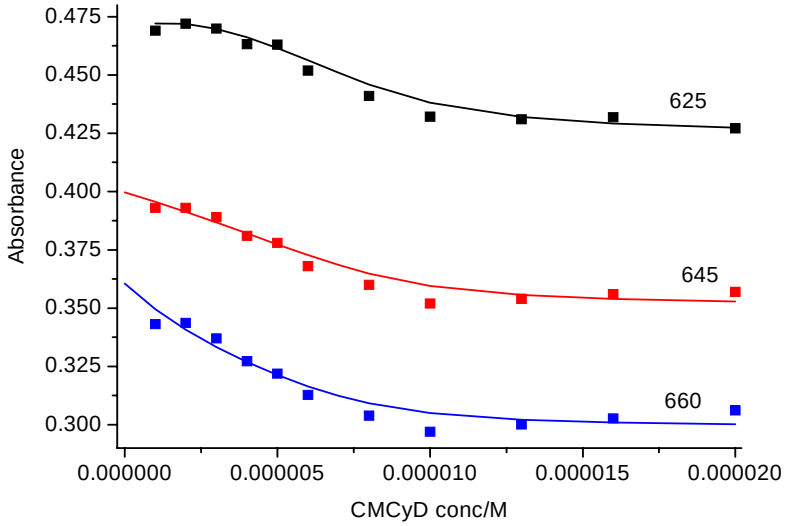

Figure S5. Global analysis of titration data of Figure 2 in the main text: comparison of experimental (symbols) and calculated (lines) absorbance at representative wavelengths (625, 645 and 660 nm), corresponding to log (K_{12}/M^{-2}) = 13.4 and log (K_{22}/M^{-3}) = 19.5 and spectra of the species in solution reported in Figure 4A of the main text.

References

1. I. Manet, F. Manoli, M. P. Donzello, E. Viola, G. Andreano, A. Masi, L. Cellai and S. Monti, *Org. Biomol. Chem.*, 2011, **9**, 684-688.
2. I. Manet, F. Manoli, M. P. Donzello, E. Viola, A. Masi, G. Andreano, G. Ricciardi, A. Rosa, L. Cellai, C. Ercolani and S. Monti, *Inorg. Chem.*, 2013, **52**, 321-328.
3. H. Gampp, M. Maeder, C. J. Meyer and A. D. Zuberbühler, *Talanta*, 1985, **32**, 257-264.
4. H. Gampp, M. Maeder, C. J. Meyer and A. D. Zuberbühler, *Talanta*, 1985, **32**, 95-101.